ACCOUNTS
of chemical research

Nonadiabatic Reaction of Energetic Molecules

ATANU BHATTACHARYA,† YUANQING GUO, AND
ELLIOT R. BERNSTEIN*

Department of Chemistry, Colorado State University, Fort Collins, Colorado

RECEIVED ON APRIL 20, 2010

CONSPECTUS

Energetic materials store a large amount of chemical energy that can be readily converted into mechanical energy via decomposition. A number of different ignition processes such as sparks, shocks, heat, or arcs can initiate the excited electronic state decomposition of energetic materials. Experiments have demonstrated the essential role of excited electronic state decomposition in the energy conversion process. A full understanding of the mechanisms for the decomposition of energetic materials from excited electronic states will require the investigation and analysis of the specific topography of the excited electronic potential energy surfaces (PESs) of these molecules. The crossing of multidimensional electronic PESs creates a funnel-like topography, known as conical intersections (CIs). CIs are well established as a controlling factor in the excited electronic state decomposition of polyatomic molecules.

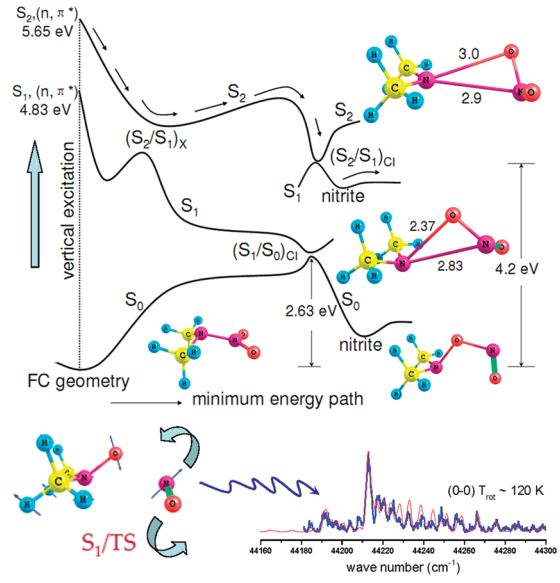

This Account summarizes our current understanding of the nonadiabatic unimolecular chemistry of energetic materials through CIs and presents the essential role of CIs in the determination of decomposition pathways of these energetic systems. Because of the involvement of more than one PES, a decomposition process involving CIs is an electronically nonadiabatic mechanism. Based on our experimental observations and theoretical calculations, we find that a nonadiabatic reaction through CIs dominates the initial decomposition process of energetic materials from excited electronic states. Although the nonadiabatic behavior of some polyatomic molecules has been well studied, the role of nonadiabatic reactions in the excited electronic state decomposition of energetic molecules has not been well investigated. We use both nanosecond energy-resolved and femtosecond time-resolved spectroscopic techniques to determine the decomposition mechanism and dynamics of energetic species experimentally. Subsequently, we employ multiconfigurational methodologies (such as, CASSCF, CASMP2) to model nonadiabatic molecular processes of energetic molecules computationally. Synergism between experiment and theory establishes a coherent description of the nonadiabatic reactivity of energetic materials at a molecular level.

Energetic systems discussed in this Account are nitramine- and furazan-based species. Both energetic species and their respective model systems, which are not energetic, are studied and discussed in detail. The model systems have similar molecular structures to those of the energetic species and help significantly in understanding the decomposition behavior of the larger and more complex energetic molecules. Our results for the above systems of interest confirm the existence of CIs and energy barriers on the PESs of interest. The presence of the CIs and barriers along the various reaction coordinates control the nonadiabatic behavior of the decomposition process. The detailed nature of the PESs and their CIs consequently differentiate the energetic systems from model systems. Energy barriers to the chemically relevant low-lying CIs of a molecule determine whether that molecule is more or less "energetic".

Published on the Web 10/08/2010 www.pubs.acs.org/acr
10.1021/ar100067f

Introduction

Energetic materials are systems that store a large amount of chemical energy that is controllable and can be converted into mechanical energy in industrial, civil, and military applications through molecular decomposition. Excited electronic states of energetic molecules, which can be easily generated by all kinds of ignition processes, such as sparks, shocks, heat, arcs, or compression waves,[1−6] have been proven to be important in the initial step of decomposition of these materials.[7−13] *Ab initio* calculations show that compression at a pressure of 30 GPa or above causes an electronic excitation equivalent to 2−5 eV,[5] which is comparable to the excitation energies of the low-lying singlet excited electronic states of energetic molecules. Therefore, UV laser excitation provides an effective means by which to study the excited state decomposition of these energetic materials. Furthermore, to understand fully the excited electronic state decomposition of energetic materials, specific topography of excited electronic state potential energy surfaces (PESs) must also be understood.

Contemporary advances in chemical dynamics have emphasized that conical intersections (CIs), which arise due to the crossing and interaction of multidimensional PESs, play an important role in excited electronic state processes of organic polyatomic molecules.[14−17] CIs enable electronically nonadiabatic reactions (processes that span multiple electronic PESs) to occur on the time scale of a vibrational period.[17] All energetic materials are polyatomic systems with complex molecular structures. Therefore, nonadiabatic reaction through CIs is expected to play an important role in the initial steps of excited electronic state decomposition of these molecules. Although nonadiabatic reaction through CIs has been well characterized and understood for a variety of chemical systems,[16] the role of nonadiabatic processes in the decomposition of energetic materials has not been well investigated. In this regard, full understanding of nonadiabatic reactions in the unimolecular decomposition of energetic molecules is of paramount importance because such detailed information at a microscopic level may be used directly or as an input for molecular dynamics simulations to gain insight into the condensed phase processes. Furthermore, if certain key unimolecular nonadiabatic steps can be identified, one can, in principle, make a material more or less sensitive or "energetic" by chemical modifications that raise or lower the activation energy barriers for these steps.

This Account presents some recent progress made in the understanding of nonadiabatic unimolecular chemistry of energetic species facilitated by CIs following electronic excitation.[18−20] The primary energetic systems discussed in this Account are nitramine- and furazan-based energetic species. In this effort, a number of model systems, which have much simpler nonenergetic molecular structures than those of the energetic systems, are first studied in detail to assist in understanding the nonadiabatic behavior of a specific moiety in an energetic system. Then, the decomposition mechanisms for more complex energetic systems are studied and compared with those of their model systems. The newest observations and results for each energetic system are highlighted and discussed individually, and a discussion and set of conclusions are presented for energetic materials in general.

Experimental Methods

Both nanosecond energy-resolved and femtosecond time-resolved spectroscopic techniques are employed to explore the decomposition mechanisms and dynamics of energetic molecules. Matrix-assisted laser desorption is used to generate gas-phase molecules of energetic materials with low vapor pressure. The mass- or energy-resolved excitation spectra of the decomposition products of energetic materials are detected by time-of-flight mass spectrometry (TOFMS) through resonance-enhanced multiphoton ionization (REMPI). Laser-induced fluorescence (LIF) spectroscopy is also used to detect some decomposition products with high vertical ionization energy. More details on the experimental equipment, such as laser systems, pulsed nozzle, signal detection, and data acquisition, are described in our previous publications.[21−23]

Mass spectra of the decomposition products help to identify the dissociation fragments from a specific sample, and energy-resolved optical spectroscopy (REMPI or LIF) provides detailed internal state (rotational and vibrational) energy distributions of a specific product. Such information clearly reflects the forces or torques that act on the departing fragments produced in the excited electronic state decomposition of energetic molecules through a unique pathway. The internal energy/state distributions of the products ultimately lead one to propose a decomposition mechanism for the energetic material. Dynamics of the decomposition reaction is measured via femtosecond time-resolved pump−probe spectroscopy.

Theoretical Methods

Theoretically, multiconfigurational methodologies, such as, complete-active-space self-consistent-field (CASSCF) and complete-active-space Møller−Plesset second-order perturbation (CASMP2) theories are used to optimize the energies and geometries at critical points [including Franck−Condon (FC)

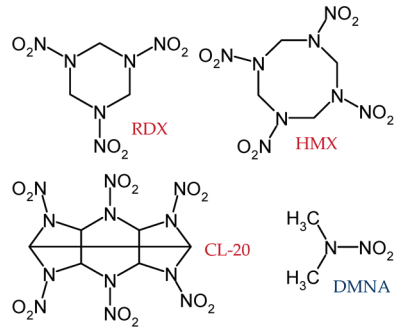

FIGURE 1. Chemical structures of RDX, HMX, CL-20, and dimethylnitramine (DMNA).

points, transition states (TSs), intermediate states, and CIs] of both model systems and energetic materials. One-dimensional minimum energy paths of multidimensional PESs are constructed based on the calculated energies and geometries at these critical points, and are used to explore the nonadiabatic molecular processes in the excited states of these molecules. Based on experimental observations and calculated PESs for a particular system, a reasonable pathway for the excited electronic state decomposition of these molecules can be proposed. All calculations are executed through the Gaussian 03 program. More details on the computational procedures and selection of active space can be found in our previous publications.[18−20] Based on the comparison of calculated FC point energies of excited states of systems of interest and their corresponding gas-phase UV absorption maxima, the accuracy of the theoretical calculations is in the range 0.1−0.5 eV.

Nonadiabatic Reactions of Nitramine (N−NO_2) Systems. Nitramine energetic materials, such as RDX (1,3,5-trinitro-1,3,5-triazacyclohexane), HMX (1,3,5,7-tetranitro-1,3,5,7-tetraazacyclooctane), and CL-20 (2,4,6,8,10,12-hexanitro-2,4,6,8,10,12-hexaazaisowurtzitane) have broad application as explosives and fuels due to their high energy content. The molecular structures of these materials are shown in Figure 1. Here, we will first present our exploration of the nonadiabatic reaction of dimethylnitramine (DMNA), a nitramine model system with a single N−NO_2 moiety;[18] we will then discuss the nonadiabatic reactions of these nitramine energetic materials based on the understanding of the DMNA model system.

DMNA. Nitric oxide (NO) is observed as a major decomposition product from dissociation of DMNA at 226 nm electronic excitation using both TOFMS and LIF spectroscopy through the resonant rovibronic transitions [$A^2\Sigma^+(v' = 0) \leftarrow X^2\Pi\ (v'' = 0)$] of NO. Only the X ($v'' = 0$) is populated. The NO product is produced through a nitro−nitrite isomerization mechanism.

$$(CH_3)_2NNO_2 \rightarrow (CH_3)_2NONO \rightarrow (CH_3)_2NO + NO$$

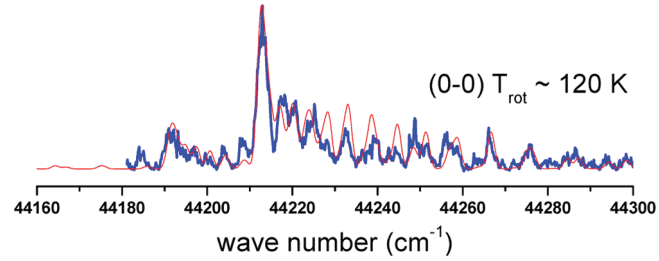

FIGURE 2. One color (1 + 1) REMPI spectrum of the vibronic transition [$A^2\Sigma^+\ (v' = 0) \leftarrow X^2\Pi\ (v'' = 0)$] of the NO product from excited electronic state decomposition of DMNA. Spectral simulation with a Boltzmann distribution (red) shows that NO from DMNA has a rotational temperature of 120 K.

The nitro−nitrite isomerization mechanism is evidenced by the observation of $(CH_3)_2NOH$ at mass channel 61 amu following 118 nm ionization of the product when DMNA is excited at 226 and 193 nm inside a quartz capillary (high collision rate) attached to the pulsed nozzle.

The OH radical is also detected to be a minor decomposition product from excited electronic state decomposition of DMNA at 226 nm excitation by LIF spectroscopy via its resonant vibronic transitions [$A^2\Sigma^+(v' = 0) \leftarrow X^2\Pi\ (v'' = 0)$] at 308 nm. The estimated yield ratio between the NO and OH products indicates that 96% of the total excited electronic state decomposition of DMNA occurs through a nitro−nitrite isomerization.

The internal (rotational and vibrational) energy distributions of the major product NO are obtained by spectral simulation of its energy-resolved spectra. As illustrated in Figure 2, the (1 + 1) REMPI spectrum of NO product from excited electronic state decomposition of DMNA at 226 nm produces a hot rotational temperature of 120 K. These rotationally hot products clearly indicate that a strong torque acts on the departing NO moiety during the dissociation of the parent molecule.

Calculations at a CASSCF(10,7)/6-31G(d) level of theory show that the electronically excited state PESs of DMNA are highly coupled along the nitro−nitrite isomerization reaction coordinate, enabling ultrafast nonadiabatic reaction to occur through this pathway. A schematic one-dimensional projection of the multidimensional singlet PESs [S_0, S_1, and S_2] of DMNA, with locations and structures of different CIs, is plotted in Figure 3, in which $(S_2/S_1)_X$ and $(S_2/S_1)_{CI}$ are CIs between S_2 and S_1 states at short and long N−N bond distances, respectively, and are localized with a (14, 11) active space including all bonding and antibonding NO orbitals. Comparison of experimental excitation energy (5.5 eV at 226 nm) with the computed vertical excitation energy implies that the

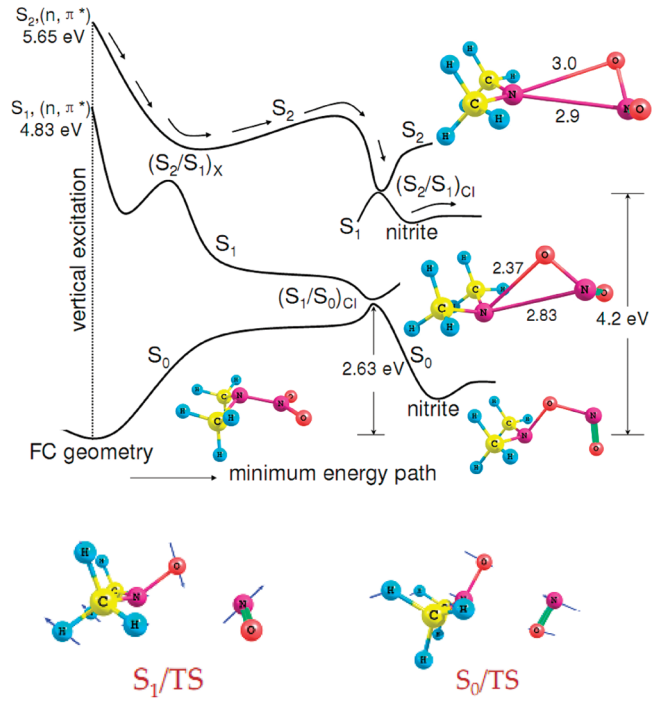

FIGURE 3. One dimensional projection of the multidimensional electronic potential energy surfaces of DMNA computed at the CASSCF(10,7)/6-31G(d) level of theory. Path arrows represent the classical trajectory of the plausible excited electronic state decomposition mechanism of DMNA. NO elimination transition states (TSs) are shown at the bottom.

DMNA molecule is excited to its S_2 state after absorbing a single 226 nm photon.

As can be seen in Figure 3, vertical excitation to the FC point of the S_2 state potentially leads to the nonadiabatic nitro−nitrite isomerization through an $(S_2/S_1)_{CI}$ CI and dimethylaminonitrite [$(CH_3)_2NONO$] on the S_1 surface will further dissociate into the NO product through the S_1/TS (transition state). The unstable normal mode of vibration for the S_1/TS transition state provides evidence of a torque acting on the NO moiety. Therefore, the nonadiabatic nitro−nitrite isomerization pathway followed by NO elimination is expected to generate rotationally hot NO product, in good agreement with the experimental observation that a rotationally hot (120 K) NO product is generated from the excited electronic state decomposition of DMNA at 226 nm (S_2).

Theoretical results also show that the nitro−nitrite isomerization occurs through the $(S_2/S_1)_{CI}$ with a loose geometry, in which the NO_2 moiety weakly interacts (∼3 kcal/mol) with the $(CH_3)_2N$ moiety from a considerably long bonding distance (∼2.8 Å). At room temperature, molecules are thermally hot (∼300 K). Therefore, hot parent molecules can provide enough vibrational energy to the intramolecular modes of DMNA that the NO_2 and $(CH_3)_2N$ moieties can diffuse away despite their initial close proximity during isomerization, resulting in NO_2 elimination as the major decomposition channel. This NO_2 elimination channel is evidenced in decomposition of DMNA at 248 and 266 nm photoexcitations at room temperature under almost collisionless conditions.[24] In a molecular beam experiment, however, molecules are extraordinarily cold (∼1 K) and thus the two moieties NO_2 and $(CH_3)_2N$ can remain in close proximity, rendering nitro−nitrite isomerization as the major decomposition channel. The same is possible even at room temperature in a dense gaseous medium, for which cage effects can again keep the two moieties in close proximity, resulting in the nitro−nitrite isomerization as a major decomposition channel. Both pathways have been observed in our experiments. These experimental condition dependent decomposition pathways for DMNA cannot be explained without consideration of nonadiabatic reactions for this molecule.

RDX, HMX, and CL-20. NO is the only observed product from excited electronic state decomposition of RDX, HMX, and CL-20 at 226−258 nm excitation;[23] its rovibronic energy distribution is different, however, than that found above for NO from nonenergetic DMNA. Additionally, the OH radical is not detected. Based on the spectroscopic signature for the NO product from RDX, HMX, and CL-20, the dissociation mechanism for these energetic molecules is proposed to be a nitro−nitrite isomerization.

The internal energy distributions of the NO product are obtained from the (1 + 1) REMPI spectra of NO from photoexcitation of these three energetic molecules in the NO $A^2\Sigma^+$ ($v' = 0$) ← $X^2\Pi$ ($v'' = 0,1,2,3$) transition region (226−258 nm). Typical spectra of the NO product from RDX with cold rotational (20 K) and hot vibrational (1800 K) distributions are displayed in Figure 4. NO products from decomposition of HMX and CL-20 show similar internal energy distribution to that from RDX. Observation of vibrationally hot (∼1800 K) NO product from excited electronic state decomposition of RDX, HMX, and CL-20 suggests that nitramine energetic molecules dissociate on their ground electronic state PESs after rapid internal conversion from upper excited electronic states.

The excited electronic state decomposition dynamics of RDX, HMX, and CL-20 can be measured by femtosecond pump−probe spectroscopy. A pump pulse at 226 nm is employed to excite and dissociate the parent molecule, and a probe pulse at the same wavelength is used to monitor the appearance of the NO product. The decomposition dynamics of these molecules are determined to be faster than 180 fs.[22] Such fast decomposition dynamics are consistent with involvement of a nonadiabatic process through a CI on their decomposition pathways.

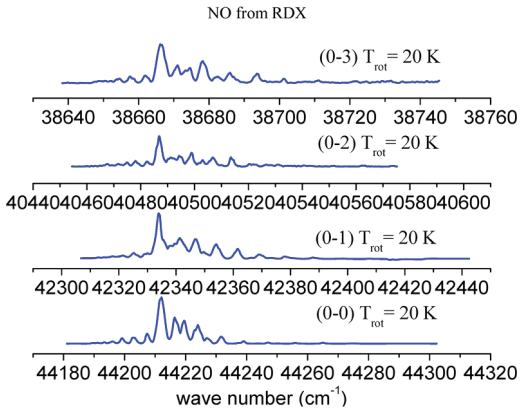

FIGURE 4. One color (1 + 1) REMPI spectra of the vibronic transitions [$A^2\Sigma^+$ ($\nu' = 0$) ← $X^2\Pi$ ($\nu'' = 0, 1, 2, 3$)] of the NO product from excited electronic state decomposition of RDX. Spectral simulations with a Boltzmann distribution show that NO from RDX has rotational and vibrational temperature of 20 and 1800 K, respectively.

For theoretical exploration of nonadiabatic decomposition behavior of RDX, HMX, and CL-20, a search of the lowest energy CI along the nitro−nitrite isomerization reaction coordinate needs to be performed. This search, however, is not presently feasible due to the requirement of a very large active space (more than 40 active orbitals including all nonbonding nσ_O, π, and bonding and antibonding σ_{NN} and σ_{NO}) in the CASSCF calculations for these molecules. Reduction of the active space does not solve the problem; rather it introduces spurious effects into the computational results. Because of these realistic challenges, vertical excitation energy for the S_1, S_2 states and the transition states on the ground electronic state (S_0) of RDX have been computed at a restricted configuration interaction using single excitation (RCIS)/6-31+G level of theory. The vertical excitation energy for the S_1 and S_2 states is calculated to be 5.59 and 6.1 eV, respectively, indicating that these energetic molecules are excited to their first excited electronic states after single photon absorption at 226 (5.5 eV) to 258 (4.8 eV) nm wavelength. The oscillator strengths for these two excited states are predicted to be 0.0001 and 0.0093, respectively. Moreover, two concerted nitro−nitrite isomerization transition states are located on the ground PES of RDX, which indicates that one RDX molecule can dissociate into three NO molecules simultaneously through these transitions states. This is in good agreement with our experimental observations that the NO ion signal intensity from nitramine energetic molecules is proportional to the number of N−NO_2 moieties. According to these experimental observations and the analysis of the PESs of the DMNA model system, we can conclude that the excited electronic state decomposition of nitramine energetic materials (RDX, HMX, and CI-20) is a nonadiabatic process and that an $(S_1/S_0)_{CI}$ CI must be involved in the nitro−nitrite isomerization pathway.

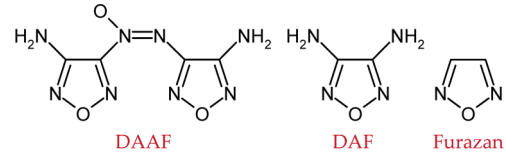

FIGURE 5. Chemical structures of DAAF, DAF, and furazan.

Comparison. Electronic excitation of RDX, HMX, and CL-20 at 226−258 nm yields a NO product that is rotationally cold (20 K) but vibrationally hot (2000 K). This observation is predicted to occur through an S_1 to S_0 internal conversion through $(S_1/S_0)_{CI}$ CI and a decomposition of the energetic material on its S_0 surface via a nitro−nitrite isomerization mechanism. Model systems such as DMNA, on the other hand, dissociate on their excited electronic state (S_1) PES with a negligible barrier (~0.1 eV) following internal conversion from S_2 to S_1 state through $(S_2/S_1)_{CI}$. Nitro−nitrite isomerization occurs through this nonadiabatic pathway, producing the NO ($X^2\Pi$) product with a hot rotational and cold vibrational distribution. Therefore, unimolecular excited electronic state decomposition of a nitramine energetic system is determined by its nonadiabatic reaction. Moreover, in order to predict molecular explosive behavior of nitramine energetic materials, knowledge of their nonadiabatic chemistry is essential.

Nonadiabatic Reactions of Furazans. Furazan-based, high nitrogen content energetic materials, especially DAAF (3,3′-diamino-4,4′-azoxyfurazan), have recently received significant attention due to their favorable properties: such properties include good heat resistivity, high heat of formation, low sensitivity, and good detonation performance for applications such as high explosives, fuels, and propellants. The structure of DAAF is illustrated in Figure 5. Here decomposition behavior of two model systems, such as diaminofurazan (DAF) and furazan (also shown in Figure 5), are also addressed for comparison.

Experimental Observations. NO is observed to be an initial decomposition product from the excited electronic state of DAAF accessed at 226, 236, and 248 nm. (1 + 1) REMPI spectra of three vibronic transitions [$A^2\Sigma^+$ ($\nu' = 0$) ← $X^2\Pi$ ($\nu'' = 0$, 1, 2)] of the NO product, shown in Figure 6, predict similar cold rotational (~20 K) distributions for three vibrational levels ($\nu'' = 0$, 1, 2) in the ground electronic state. The vibrational temperature of the NO product from DAAF is estimated to be ca. 1260 K.

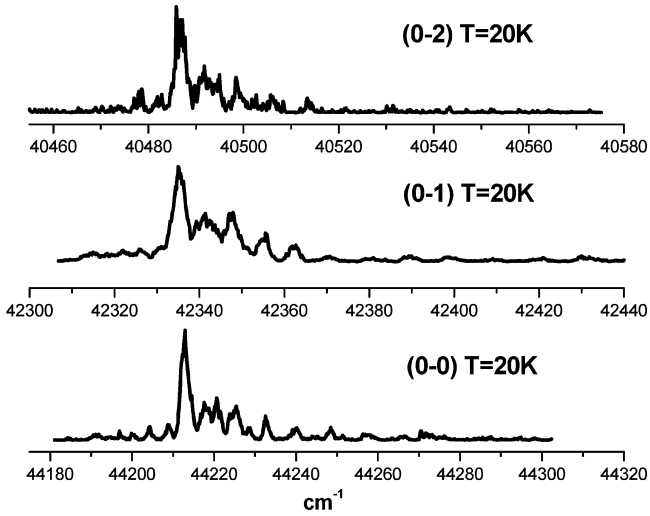

FIGURE 6. One-color (1 + 1) REMPI spectra of the vibronic transitions [$A^2\Sigma^+$ ($\nu' = 0$) ← $X^2\Pi$ ($\nu'' = 0, 1, 2$)] of the NO product from excited electronic state decomposition of DAAF. Spectral simulations with a Boltzmann distribution show that the three observed vibrational levels on the ground electronic states have a similar rotational temperature of 20 K.

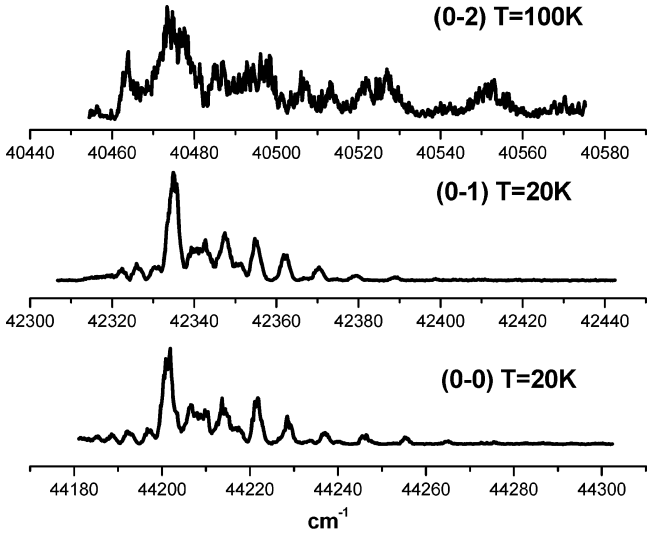

FIGURE 7. One-color (1 + 1) REMPI spectra of the vibronic transitions [$A^2\Sigma^+$ ($\nu' = 0$) ← $X^2\Pi$ ($\nu'' = 0, 1, 2$)] of the NO product from excited electronic state decomposition of DAF. Spectral simulations with a Boltzmann distribution show that the $\nu'' = 0$ and 1 vibrational levels on the ground electronic state have a similar rotational temperature of 20 K and that the $\nu'' = 2$ vibrational level has a rotational temperature of 100 K.

The (1 + 1) REMPI spectra of three vibronic transitions, $A^2\Sigma^+$ ($\nu' = 0$) ← $X^2\Pi$ ($\nu'' = 0,1,2$) of the NO product from excited electronic state decomposition of DAF are shown in Figure 7. The (0−0) and (0−1) vibronic bands of the NO product, which are detected at wavelengths of 226 and 236 nm, respectively, show a similar cold (20 K) rotational distribution to that from DAAF. On the contrary, the (0−2) vibronic band of the NO product obtained from decomposition of DAF

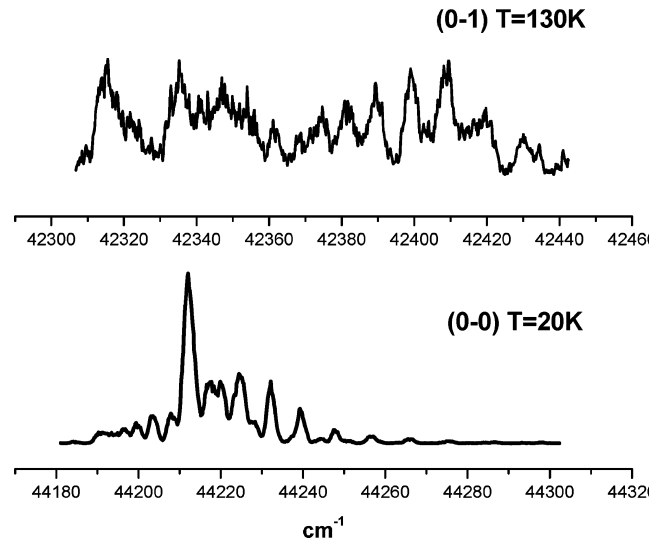

FIGURE 8. One-color (1 + 1) REMPI spectra of the vibronic transitions $A^2\Sigma^+$ ($\nu' = 0$) ← $X^2\Pi$ ($\nu'' = 0, 1$)] of the NO product from excited electronic state decomposition of furazan. Spectral simulations with a Boltzmann distribution show that the $\nu'' = 0$ vibrational level on the ground electronic states have a rotational temperature of 20 K and that the $\nu'' = 1$ vibrational level has a rotational temperature of 130 K.

accessed at 248 nm displays a much hotter rotational temperature of about 100 K.

Excited electronic state decomposition of furazan generates NO with only $\nu'' = 0$ and 1 populations. The spectra of the (0−0) and (0−1) vibronic bands of the NO product, illustrated in Figure 8, yields a cold (20 K) rotational distribution, which is similar to the (0−0) band of the NO product form DAAF and DAF; however, the (0−1) vibronic band shows a hotter rotational distribution with a temperature of about 130 K.

Based on direct comparisons of the experimental internal energy distributions of the NO products from excited electronic state decomposition of DAAF, DAF, and furazan, one can conclude that DAAF decomposes through a pathway that is independent of excitation wavelength because it only produces an NO molecule with similar cold rotational distributions (20 K) at all three excitation wavelengths (226, 236, and 248 nm). On the other hand, furazan model systems (DAF and furazan) decompose through excitation energy dependent channels, because the internal energy distributions of the NO products from these model systems vary with excitation wavelength.

Theoretical Predictions. Calculations using a CASMP2//CASSCF/6-31G(d) theory level predict two different possible nonadiabatic pathways for excited electronic state decomposition of DAF and furazan: (a) ring contraction through $(S_1/S_0)_{Cl,a}$ and (b) ring-opening through $(S_1/S_0)_{Cl,b}$.[19] A schematic

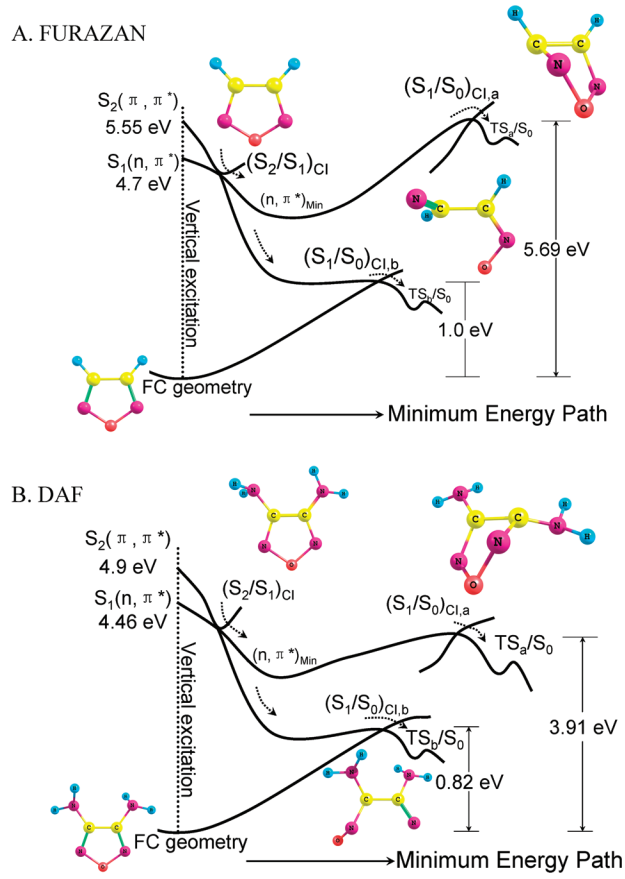

FIGURE 9. One dimensional projections of multidimensional potential energy surfaces of furazan (A) and DAF (B) computed at CASSCF/6-31G* level of theory. Energies of the critical points and conical intersections are computed at CASMP2//CASSCF/6-31G* level of theory. The branching space formed by the gradient difference and derivative coupling vectors are not calculated here. Instead, the minimum energy paths leading to $(S_1/S_0)_{CI,a}$ and $(S_1/S_0)_{CI,b}$ are calculated by running an IRC calculation from respective CIs in a backward direction using the initial force constants calculated at the respective CIs. Two nonadiabatic dissociation channels along two different nuclear coordinates are indicated by dotted arrows. See text for further details.[19]

one-dimensional projection of the multidimensional PESs of furazan and DAF are plotted in Figure 9A,B, respectively. Surfaces are computed at a CASSCF/6-31G* theory level and the critical points on the surfaces are computed at the CASMP2//CASSCF/6-31G* theory level.

Figure 9 A shows that the furazan molecule is excited to its $S_2(\pi,\pi^*)$ electronic state after absorbing a single photon at 226 (5.49 eV) or 236 nm (5.26 eV), as used in the experiments.[19] The $(S_1/S_0)_{CI,a}$ IC on the PESs of furazan is located at a similar energy (within an energy uncertainty of ~0.1 eV, the difference between the computed FC point energy of excited state at CASMP2//CASSCF level of theory for furazan and the corresponding gas-phase UV absorption maximum) to that of the absorption maximum of the spectroscopically active $S_2(\pi,\pi^*)$ state. Therefore, following electronic excitation to the $S_2(\pi,\pi^*)$ state of furazan at 226 nm (5.49 eV), the molecule can access a ring contraction nonadiabatic pathway from the FC point of its $S_2(\pi,\pi^*)$ state though $(S_1/S_0)_{CI,a}$ after crossing the $(S_2/S_1)_{CI}$ CI. Following this pathway, furazan relaxes back to the ground state and dissociates through an NO elimination pathway. The transition state (TS) associated with NO elimination on the ground electronic surface possesses an unstable vibrational mode presenting a NO−azirene (C_2H_2N) symmetric stretch. Since the NO moiety for this NO elimination TS experiences little torque, one can predict that the NO product from furazan following 226 nm excitation should be rotationally cold, consistent with the experimental observation.

On the other hand, furazan cannot surmount the energy barrier for the $(S_1/S_0)_{CI,a}$ CI when it is excited at 236 nm (5.26 eV) since this excitation energy is about 0.43 eV lower than the energy barrier on the pathway to the $(S_1/S_0)_{CI,a}$ CI. Instead, electronic excitation at 5.26 eV is predicted to lead the molecule to the $(S_1/S_0)_{CI,b}$ after crossing the $(S_2/S_1)_{CI}$ CI. This nonadiabatic pathway is associated with a ring-opening mechanism and finally brings the molecule to the ground state. Consequently, the excited furazan molecule dissociates through a NO elimination pathway on its ground electronic state. This pathway will produce a NO product with a hot rotational distribution because the NO elimination TS on the ground electronic state surface following the $(S_1/S_0)_{CI,b}$ CI is associated with an unstable normal mode of vibration imparting a torque on the NO moiety. Thus, calculations suggest that excited electronic state decomposition of furazan at 5.49 eV (226 nm) and 5.26 eV (236 nm) electronic excitations involves two different nonadiabatic dissociation pathways: one yielding rotationally cold NO as initial decomposition product through $(S_1/S_0)_{CI,a}$ CI, and another generating rotationally hot NO as initial decomposition product through $(S_1/S_0)_{CI,b}$ CI.

For DAF, the absorption maximum energy of the spectroscopically active $S_2(\pi,\pi^*)$ state is calculated to be 4.9 eV at the CASMP2//CASSCF/6-31G* level of theory, which is ~0.5 eV lower than the experimental absorption maximum value (obtained in methanol solution) of ~5.4 eV. A direct comparison of the computed and experimental absorption energies for DAF is therefore not very relevant or valuable. Rather a qualitative comparison of the relative position of the CIs with respect to the FC point of the $S_2(\pi,\pi^*)$ state of this molecule is a more appropriate and useful comparison to draw. The $(S_1/S_0)_{CI,a}$ CI on the PESs of DAF (see Figure 9B) is predicted to be lower in energy than the vertical excitation energy of the $S_2(\pi,\pi^*)$ state. [Note that for furazan a similar $(S_1/S_0)_{CI,a}$ CI is predicted to be at roughly the same energy as that of the FC

point.] This renders the $(S_1/S_0)_{CI,a}$ CI for DAF energetically accessible from even much below the FC point of its $S_2(\pi,\pi^*)$ state. Thus, electronic excitation of DAF at 226 (5.46 eV) and 236 nm (5.26 eV) follows the ring contraction nonadiabatic pathway through $(S_1/S_0)_{CI,a}$ CI, which produces NO products with cold rotational distributions. Decomposition of DAF at 248 nm [5.00 eV, below its $(S_1/S_0)_{CI,a}$ CI], however, follows a different pathway generating rotationally hot distributions for the NO product. This latter pathway undoubtedly involves a ring-opening mechanism through the $(S_1/S_0)_{CI,b}$ CI.

Therefore, the CASMP2//CASSCF/6-31G* level of theory predicts two different decomposition pathways for DAF consistent with experimental observation. This level of theory, however, places the $(S_1/S_0)_{CI,a}$ CI too low in energy with respect the FC point of the $S_2(\pi,\pi^*)$ state for DAF according the experimental results quoted above. The energy difference between the FC point of the $S_2(\pi,\pi^*)$ state and the $(S_1/S_0)_{CI,a}$ CI is predicted to be ~1 eV (the energy uncertainty of the computation is ~0.5 eV for DAF) at the CASMP2//CASSCF/6-31G* level of theory. Because experimental observation reveals that electronic excitation of DAF at 236 nm (5.26 eV) generates rotationally cold distribution of the NO and that at 248 nm (5.0 eV) produces rotationally hot distribution of the NO, we predict that the actual energy difference between the FC point of the $S_2(\pi,\pi^*)$ state and the $(S_1/S_0)_{CI,a}$ CI has to be ~0.4 eV. Further improvement of the level of theory could be done by selecting a larger active space for DAF.

Comparison. The excited electronic state decomposition of furazan-based model systems (furazan and DAF) follows excitation wavelength dependent dissociation channels. These pathways are the result of their specific nonadiabatic reactions through different CIs connecting different electronic states. On the other hand, excited electronic state decomposition of DAAF follows a single excitation wavelength independent dissociation channel. A similar single excitation wavelength independent dissociation channel is also observed from RDX, HMX, and CL-20. In these systems, dissociation occurs on the S_0 surface through a series of CIs involving $S_2 \rightarrow S_1 \rightarrow S_0$ internal conversion. This process provides a barrierless single decay channel for decomposition from excited electronic states.

Detailed theoretical exploration of nonadiabatic reactions for DAAF is not possible using current computational capabilities due to the required large active space. Nonetheless, experimental observations provide a number of important insights about the nonadiabatic decomposition of DAAF. In comparison with model systems, such as DAF and frurazan, we can suggest that rotationally cold distributions of the NO product from DAAF are generated through the ring contraction mechanism through a similar $(S_1/S_0)_{CI,a}$ CI to that found for DAF and furazan. Furthermore, the $(S_1/S_0)_{CI,a}$ CI in the ring contraction reaction coordinate on the PESs of DAAF should be located at an energy much lower than the FC point of excited state surfaces so that it can be readily accessed by electronic excitations at all three excitation wavelengths used in our experiments. The model systems, on the other hand, decompose through different pathways dependent on excitation energy. Thereby, the relative position of the energy barrier for the $(S_1/S_0)_{CI,a}$ CI in the ring contraction reaction coordinate with respect to the excitation energy plays a crucial role in the decomposition mechanism of these molecules.

General Discussion and Conclusions

Based on the analysis of excited electronic state decomposition mechanisms for two different categories of energetic materials and model systems (nitramine and furazan), we present a complex but clear picture to illustrate the important role of nonadiabatic reactions involving CIs in the excited electronic state decomposition of high energy content materials. CIs, a crossing between adiabatic electronic PESs, have been proven to be ubiquitous in all systems of interest and play a central role in excited electronic state decomposition channels of these materials. The unique decomposition pathway that results in different decomposition products with characteristic internal energy distributions for each individual molecule is determined and controlled not only by the number of the CI but also by the energy barriers for these intersections on the final diabatic PESs. For example, the presence of CIs in the nitro−nitrite isomerization reaction coordinate of nitramines leads to nonadiabatic decomposition of nitramines along this pathway following $(\pi^* \leftarrow n)$ or $(\pi^* \leftarrow \pi)$ electronic excitations. The nitramine model system (DMNA) dissociates on its excited electronic state surface following internal conversion from S_2 to S_1 through an $(S_2/S_1)_{CI}$ CI and produces an NO product with hot rotational but cold vibrational distributions. Nitramine energetic materials (RDX, HMX, and CL-20), on the other hand, undergo excited electronic state decomposition on their ground electronic state surfaces after internal conversion from excited electronic states through CIs; they produce NO products with cold rotational and hot vibrational distributions. Furthermore, furazan-based model molecules dissociate through two different decomposition pathways, both of which are electronically nonadiabatic. Energy barriers for the CIs with respect to the excitation energy control the overall excited electronic state decomposition of furazan based model systems: they dissociate either through a ring

contraction mechanism if the excitation energy is greater than the energy barrier for this channel or through a ring-opening mechanism if the excitation energy is less than that required for the ring contraction channel. Therefore, these results might be an indication of the quality of an energetic material and present a way for synthetic chemists to make predictions and judgments for the design and synthesis of better energetic materials.

For larger energetic materials, one can suggest that the excited electronic state decomposition of all energetic materials follow nonadiabatic pathways through CIs. Due to the dissociative nature of the excited states of energetic materials through multiple PESs and their couplings, no energy barrier exists for the decomposition of energetic materials through CIs. This mechanism results in a unique excitation energy independent pathway to convert the stored chemical energy into mechanical energy during the decomposition process that eventually occurs on the ground electronic state PES.

One of the most important implications of a CI for the chemistry of energetic materials is rapid and efficient internal conversion from upper to lower electronic state PESs through radiationless transitions. This internal conversion facilitates rapid conversion of electronic energy (produced from an initiation pulse), belonging to the upper electronic state, to vibrational energy of the lower electronic state, with a potential time scale of a few femtoseconds. Therefore, the presence of CIs in the decomposition pathways of energetic materials makes the initial step in the excited electronic state decomposition of energetic materials ultrafast (faster than 180 fs). Dynamics of these decompositions is controlled by the nonadiabatic coupling between different excited electronic potential energy surfaces, which is dependent upon the energy differences between the involved adiabatic states. Further quantitative calculations on the nonadiabatic dynamics and the branching ratios of the excited electronic state decomposition of energetic materials and model systems could be performed by the on-the-fly surface-hopping simulation methods, which have been employed to simulate the nonadiabatic photodynamics of many organic systems.[25,26]

In a brief summary, this Account presents an enhanced understanding of the critical role of nonadiabatic couplings in the initial steps of the excited electronic state decomposition of energetic materials. In addition, it provides a potentially useful methodology for accurate and predictive determination, design, and synthesis of new energetic materials.

This work is supported in part by grants from the U.S. ARO.

BIOGRAPHICAL INFORMATION

Atanu Bhattacharya achieved his Ph.D. at Colorado State University (E. R. Bernstein) in 2009. His Ph.D. work involved understanding the mechanism and dynamics of decomposition of energetic materials. He is currently a research associate in department of chemistry at Brookhaven National Lab (Nick Camillone III).

Yuanqing Guo received his Ph.D. degree in atomic and molecular physics from WIPM, the Chinese Academy of Sciences, in 2001. He worked as a Postdoctoral Fellow with Dr. Temps for two years in the Institute of Physical Chemistry at Kiel University, Germany. He joined Dr. Bernstein's research group in 2003 and has been working on projects involving mechanisms and dynamics of decomposition of energetic materials.

Elliot R. Bernstein received his Ph.D. degree from Caltech (G. W. Robinson). He was a Fermi Postdoctoral Fellow at the University of Chicago (C. A. Hutchison, Jr.). He has been on the faculty of Colorado State University since 1975. His present research interests are metal and metal compound cluster catalytic chemistry, structure and dynamics of neutral and ionic bioactive molecules, and the decomposition mechanisms and dynamics of energetic materials.

FOOTNOTES

† Current address: Chemistry Department, Brookhaven National Lab, Upton, NY 11961, U.S.A.

REFERENCES

1 Bernstein, E. R. In *Overviews of Recent Research on Energetic Materials*; Thompson, D., Brill, T., Shaw, R., Eds.; World Scientific, Hackensack, NJ, 2004.

2 Williams, F. E. Electronic states of solid explosives and their probable role in detonations. *Adv. Chem. Phys.* **1971**, *21*, 289–302.

3 Sharma, J.; Beard, B. C.; Chaykovsky, M. Correlation of impact sensitivity with electronic levels and structure of molecules. *J. Phys. Chem.* **1991**, *95*, 1209–1213.

4 Gilman, J. Chemical reactions at detonation fronts in solids. *J. Philos. Mag. B* **1995**, *71*, 1057–1068.

5 Kuklja, M. M.; Aduev, B. P.; Aluker, E. D.; Krasheninin, V. I.; Krechetov, A. G.; Mitrofanov, A. Y. Role of electronic excitations in explosive decomposition of solids. *J. Appl. Phys.* **2001**, *89*, 4156–4166.

6 Windawi, H. M.; Varma, S. P.; Cooper, C. B.; Williams, F. Analysis of lead azide thin films by Rutherford backscattering. *J. Appl. Phys.* **1976**, *47*, 3418–3420.

7 Schanda, J.; Baron, B.; Williams, F. Luminescence of lead azide. *Acta Tech. Acad. Sci. Hung.* **1975**, *80*, 185–192.

8 Schanda, J.; Baron, B.; Williams, F. Low-temperature photoluminescence of lead azide. *J. Lumin.* **1974**, *9*, 338–342.

9 Varma, S. P.; Williams, F. Infrared absorption spectra of doped and undoped lead azide. *J. Chem. Phys.* **1973**, *59*, 912–915.

10 Hall, R. B.; Williams, F. Photodecomposition and electronic structure of lead azide. *J. Chem. Phys.* **1973**, *58*, 1036–1042.

11 Dremin, A. N.; Klimenko, V. Y.; Davidoua, O. N.; Zolodeva, T. A. *Proc. 9th Symp. Detonation, Portland OR* **1989**, 319.

12 Sharma, J.; Forbes, J. W.; Coffey, C. S.; Liddiard, T. P. Infrared spectroscopy of carbo-ions. V. Classical vs nonclassical structure of protonated acetylene $C_2H_3^+$. *J. Phys. Chem.* **1987**, *91*, 5139–5153.

13 Sharma, J. Presented at the APS Topical Meeting on Shocks in Energetic Materials; Williamsburg VA, 1991.

14 Levine, R. D. *Molecular Reaction Dynamics*; Cambridge University Press: Cambridge, UK, 2005, p 264.

15 Worth, G. A.; Cederbaum, L. S. BEYOND BORN-OPPENHEIMER: Molecular dynamics through a conical intersections. *Annu. Rev. Phys. Chem.* **2004**, *55*, 127–158.

16 Domcke, W.; Yarkony, D. R.; Koppel, H. *Conical Intersections: Electronic Structure, Dynamics and Spectroscopy*; World Scientific: Hackensack, NJ, 2003.

17 Baer, M.; Billing, G. D. The role of degenerate states in chemistry. *Adv. Chem. Phys.* **2002**, *124*, 39–142.

18 Bhattacharya, A.; Guo, Y. Q.; Bernstein, E. R. Experimental and theoretical exploration of the initial steps in the decomposition of a model nitramine energetic material: Dimethylnitramine. *J. Phys. Chem. A* **2009**, *113*, 811–823.

19 Guo, Y. Q.; Bhattacharya, A.; Bernstein, E. R. Excited electronic state decomposition of furazan based energetic materials: 3,3′-Diamino-4,4′-azoxyfurazan and its model system, diaminofurazan and furazan. *J. Chem. Phys.* **2008**, *128*, 034303.

20 Bhattacharya, A.; Guo, Y. Q.; Bernstein, E. R. Unimolecular decomposition of tetrazine-N-oxide based high nitrogen content energetic materials from excited electronic states. *J. Chem. Phys.* **2009**, *131*, 194304.

21 Guo, Y. Q.; Greenfield, M.; Bernstein, E. R. Decomposition of nitramine energetic materials in excited states: RDX and HMX. *J. Chem. Phys.* **2005**, *122*, 244310.

22 Greenfield, M.; Guo, Y. Q.; Bernstein, E. R. Ultrafast photodissociation dynamics of HMX and RDX from their excited electronic states via femtosecond laser pump-probe techniques. *Chem. Phys. Lett.* **2006**, *430*, 277–281.

23 Guo, Y. Q.; Greenfield, M.; Bernstein, E. R. On the excited electronic state dissociation of nitramine energetic materials and model systems. *J. Chem. Phys.* **2007**, *127*, 154301.

24 McQuaid, M. J.; Miziolek, A. W.; Sausa, R. C.; Merrow, C. N. Dissociation of dimethylnitramine at 248 nm. *J. Phys. Chem.* **1991**, *95*, 2713–2718.

25 Barbatti, M.; Granucci, G.; Persico, M.; Ruckenbauer, M.; Vazdar, M.; Eckert-Maksic, M.; Lischka, H. The on-the-fly surface-hopping program system Newton-X application of ab initio simulation of the nonadiabatic photodynamics of benchmark systems. *J. Photochem. Photobiol. A: Chem.* **2007**, *190*, 228–240.

26 Lan, Z.; Fabiano, E.; Thiel, W. Photoinduced nonadiabatic dynamics of pyrimidine nuclearbases: On-the-fly surface-hopping study with semiemperical methods. *J. Phys. Chem. B* **2009**, *113*, 3548–3555.